CrossMark

ADVANCED REAL TIME OPTICAL IMAGING

# Quantitative and Qualitative Aspects of Gas–Metal–Oxide Mass Transfer in High-Temperature Confocal Scanning Laser Microscopy

STEPHANO P.T. PIVA,[1,2] P. CHRIS PISTORIUS ◉,[1,3]
and BRYAN A. WEBLER[1]

1.—Department of Materials Science and Engineering, Center for Iron and Steelmaking Research, Carnegie Mellon University, 5000 Forbes Avenue, Pittsburgh, PA 15213, USA. 2.—CAPES Foundation, Ministry of Education of Brazil, Brasília, DF 70040-020, Brazil. 3.—e-mail: pistorius@cmu.edu

During high-temperature confocal scanning laser microscopy (HT-CSLM) of liquid steel samples, thermal Marangoni flow and rapid mass transfer between the sample and its surroundings occur due to the relatively small sample size (diameter around 5 mm) and large temperature gradients. The resulting evaporation and steel–slag reactions tend to change the chemical composition in the metal. Such mass transfer effects can change observed nonmetallic inclusions. This work quantifies oxide–metal–gas mass transfer of solutes during HT-CSLM experiments using computational simulations and experimental data for (1) dissolution of MgO inclusions in the presence and absence of slag and (2) Ca, Mg–silicate inclusion changes upon exposure of a Si–Mn-killed steel to an oxidizing gas atmosphere.

## INTRODUCTION

High-temperature confocal scanning laser microscopy has been used extensively to study high-temperature reactions on liquid metals and slags, and at the interfaces between liquid metal and transparent slag. Because of the small sample size (typically a few millimeters in diameter), mass transfer from and within the sample is fast, and can significantly affect the observed reactions, especially if the sample contains species with relatively high vapor pressures (such as Mn and Mg) or if volatile species (such as SiO and CO) can form by reaction. This work analyzes experimental examples of such effects, with simulation of mass transfer within a molten sample. Previous work showed that gas-phase mass transfer from hemispherical liquid droplets in HT-CSLM experiments can be approximated as diffusion into a static medium, with Sherwood number of $Sh = 2$.[1]

The first case presented in this work deals with mass transfer within a liquid metal droplet. Thermal and solutal gradients in the metal drive fluid flow, sometimes leading to surface instability and self-emulsification.[2–4] These flow phenomena are commonly observed during study of interaction, agglomeration, and coalescence of buoyant nonmetallic inclusions on metal droplets.[5–8]

The Bond number ($Bo$) compares the magnitude of gravitational forces with surface tension. To evaluate the effect of the temperature gradient in fluid flow, the modified Bond number ($Bo'$) is calculated using the temperature coefficients of surface tension and density of molten iron instead of density and surface tension. The coefficient for density is $(\partial \rho / \partial T) = -0.836$ kg/m³K and for surface tension is $(\partial \sigma / \partial T) = -0.00034$ N/mK.[9] The calculated modified Bond number is $Bo' = 0.15$, for a radius $L = 2.5$ mm in an inert crucible at 1873 K; see Eq. 1.[10] Since $Bo' < 1$, the dominant force for fluid flow is surface tension and not buoyancy. The results of computational fluid dynamics simulations (presented below) confirm this conclusion.

In these calculations, equilibrium conditions (boundary conditions for mass transfer) were calculated using FactSage 7.1,[11] using the liquid iron solution model from the FTmisc database, and models for slag and solid oxides from the FToxid database.

$$Bo' = \frac{\left(\frac{\partial \rho}{\partial T}\right)gL^2}{\left(\frac{\partial \sigma}{\partial T}\right)} = 0.15. \qquad (1)$$

## CASE 1: EFFECT OF Mg EVAPORATION ON IN SITU OBSERVATION OF MgO INCLUSIONS IN HIGH-Al STEELS

Kumar and Pistorius[12] demonstrated Mg evaporation from the free surface of liquid aluminum-killed steel in contact with MgO-saturated slag in HT-CSLM; Mg evaporation led to MgO whisker growth on the crucible wall. In another example of the effect of gas–steel–slag–inclusion mass transfer, Mu et al.[8] observed that MgO inclusions at the surface of molten Fe-0.16%Al alloys disappeared during HT-CSLM if the sample was contained in an MgO crucible; if an MgO-saturated calcium aluminate slag surrounded the steel droplet, inclusions did not vanish (see Fig. 1 for the approximate geometries of these two experiments). Disappearance of the MgO inclusions was ascribed to vaporization of Mg from the free surface of the metal droplet, causing dissolution of MgO into the steel; the rate-determining step for inclusion dissolution appeared to be mass transfer from the inclusions at the (Mg-depleted) steel surface. In the presence of slag, the supply of Mg to the steel (from reduction of MgO from the slag, by Al dissolved in the steel) was apparently sufficiently rapid to maintain inclusion stability at the metal surface, or at least retard dissolution greatly.

### Calculation Approach

To quantify fluid flow and heat transfer in a typical HT-CSLM setup, two two-dimensional (2D) axisymmetric geometries (droplet–crucible and droplet in slag; Fig. 1) were simulated using COMSOL Multiphysics 5.2, solving the laminar flow, heat transfer, and transport of dilute species equations.

Concentration boundary conditions were imposed by local equilibrium at the steel–crucible interface and steel–slag interface (if present). In the presence of MgO-saturated CaO–MgO–Al$_2$O$_3$ slag (as used in the simulated experiments), [Mg]$_{interface}$ = 19 ppm (by mass) for Fe-0.16%Al steel (calculated with FactSage). For experiments without slag, magnesium spinel formed[8] at the droplet–crucible interface, reflecting a higher alumina activity in the system; the calculated [Mg] is 13 ppm for MgO–spinel steel equilibrium (Fig. 2). The temperature was fixed at the bottom of the crucible, and it was assumed that radiation occurred at all surfaces (Fig. 1). The crucible–steel interface was assumed to be a no-slip plane, whereas the steel–gas and steel–slag interfaces were slip planes. The evaporative flux was calculated from the molar concentration of magnesium at the steel surface using Eq. 2, in which $K_{vap,i}$ is the equilibrium constant for evaporation with a 1% reference state in molten iron.[9] The gas-phase Sherwood number around a
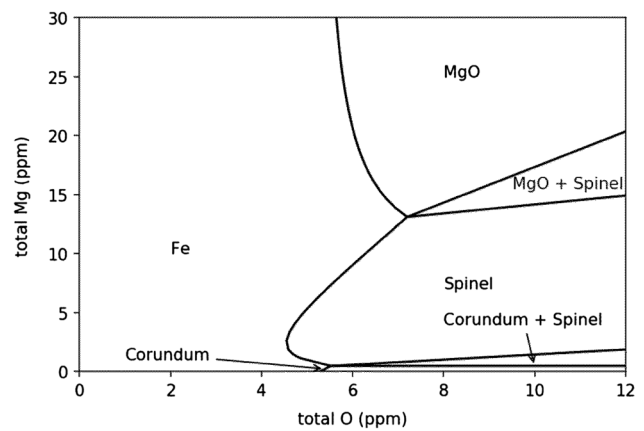
Fig. 2. Stability diagram of oxides depending on Mg and O concentrations for Fe-0.16%Al alloy at 1600°C, calculated with FactSage 7.1.
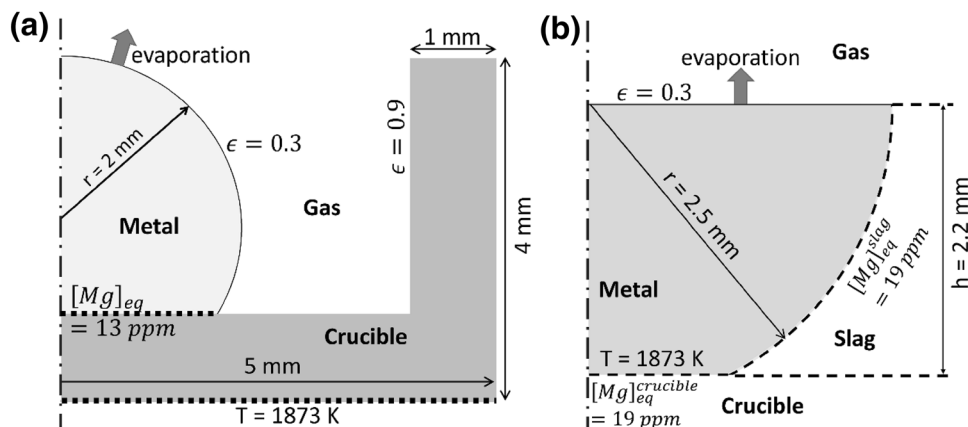
Fig. 1. Schematics of assumed boundary conditions for the flow, heat, and mass transfer problems: (a) droplet–crucible geometry and (b) droplet-in-slag geometry.

Quantitative and Qualitative Aspects of Gas–Metal–Oxide Mass Transfer in High-Temperature Confocal Scanning Laser Microscopy

1195

hemispherical HT-CSLM sample is 2.[1] The mass transfer coefficient $k_{gas}$ was then calculated, with the diffusivity of Mg in Ar gas ($D_{Mg,gas} = 1.4 \times 10^{-4} m^2/s$) based on its molar volume and boiling point.[13]

$$\frac{1}{A}\frac{dN_i}{dt} = k_{gas}\left(K_{vap,i}\frac{M_i}{\rho_{Fe}}C_i \times 100\%\right) \times 101,325. \quad (2)$$

Fluid properties used in the calculation were for liquid iron. The temperature dependence of surface tension ($\sigma$), density ($\rho$), and dynamic viscosity ($\mu$) (Eqs. 3–5) was taken from literature, with $k = 35$ W/mK (thermal conductivity), $C_p = 824$ J/mol K (heat capacity),[9] and $D_{Mg} = 5 \times 10^{-9}$ m$^2$/s (diffusivity of Mg in molten iron).[14]

$$\sigma/[N/m] = 2.367 - 0.00034(T/[K] - 273.15), \quad (3)$$

$$\rho/[kg/m^3] = 8300 - 0.836(T/[K] - 273.15), \quad (4)$$

$$\log(\mu/[Pa\ s]) = -3.479 + \frac{2324.8}{T/[K]}. \quad (5)$$

## Results and Discussion

Simulation results in Fig. 3a and d show that the calculated temperature difference over the height of the droplet is approximately 30 K without slag, and 20 K with slag. These temperature differences lead to surface-tension-driven rolling flow patterns (Fig. 3b and e). Without slag, the maximum speed is $4.8 \times 10^{-2}$ m/s at the droplet surface (Fig. 3b); with slag, the maximum speed is $2.5 \times 10^{-2}$ m/s at the free surface and $1.8 \times 10^{-2}$ m/s at the steel–slag interface (Fig. 3e). The smaller temperature difference and lower speeds in the presence of slag result from the smaller radiating steel surface.

Much larger differences in steady-state concentrations of Mg are found between the two cases (Fig. 3c and f). In the absence of slag, the average concentration at the steel surface is 0.35 mol/m$^3$ (1.2 ppm Mg), much lower than the value of 3 mol/m$^3$ (10 ppm Mg) in the presence of slag. The much higher surface concentration in the latter case would lead to much slower dissolution of MgO inclusions, as observed experimentally.[8] The higher surface concentration in the presence of slag is the result of the larger surface—steel–crucible and steel–slag—supplying dissolved Mg (at a higher equilibrium concentration), and a smaller free steel surface (for evaporation). In both cases, the [Mg] differences within the steel droplet support the conclusion that steel mass transfer (and not gaseous mass transfer) limits the rate of Mg vaporization.[8]

## CASE 2: GAS-PHASE MASS TRANSFER TO AND FROM A Si–Mn-KILLED STEEL DROPLET

Reoxidation of previously deoxidized liquid steel can be used to detect the presence of low concentrations of elements with high affinity for oxygen. As an example, magnesium spinel inclusions often form upon reoxidation of calcium-treated aluminum-killed steel, revealing dissolved magnesium at a concentration of a few parts per million.[15]

A lollipop sample taken from liquid steel was obtained from an industrial steel processing route that desulfurizes Si-killed steel using a CaO–CaF$_2$–SiO$_2$–MgO slag.[16] In this process, a low SiO$_2$ activity in the slag leads to highly reducing conditions (resulting in deep desulfurization). Strong stirring (in a tank degasser) and double saturation by CaO and MgO are expected to result in relatively high concentrations of dissolved Ca and Mg in steel. Given that the concentrations of dissolved Ca and Mg in liquid steel under industrial conditions
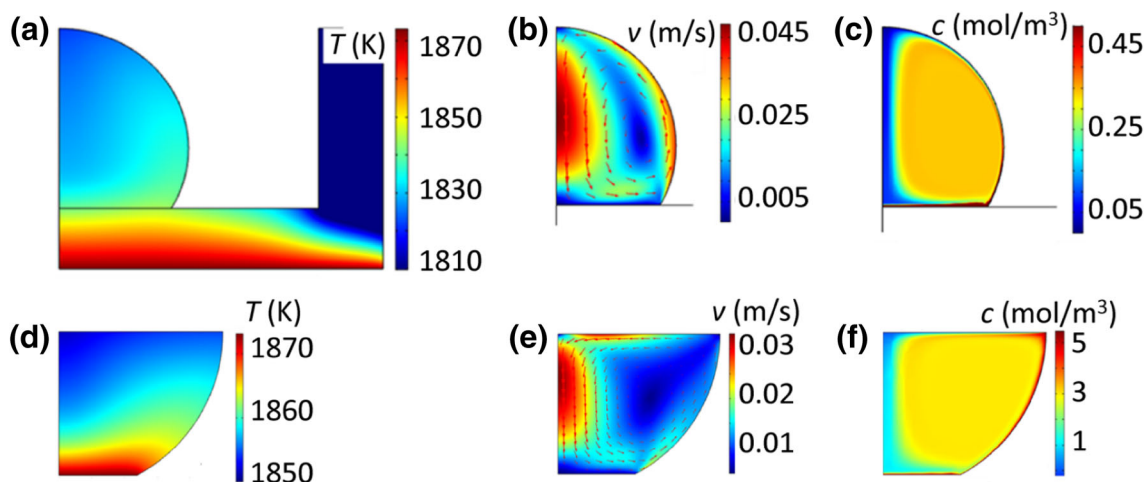


Fig. 3. COMSOL Multiphysics simulation results for Marangoni flow in steel droplets in HT-CSLM: (a–c) without slag (geometry of Fig. 1a) and (d–f) with slag (geometry of Fig. 1b).
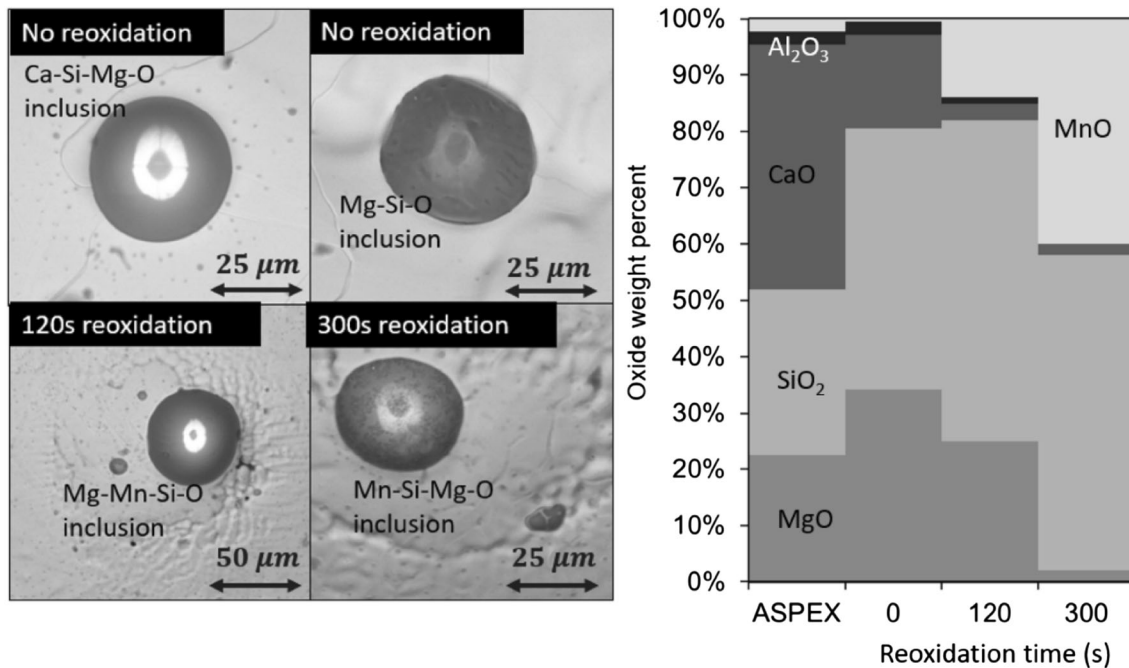
Fig. 4. Secondary-electron images of nonmetallic inclusion agglomerate located at the center of solidified HT-CSLM samples, for oxidation times as labeled. The overall chemical composition of the inclusions is given at right; the column marked "ASPEX" refers to inclusions present before reoxidation.

remain poorly known, these appeared to be appropriate samples for reoxidation—to assess whether dissolved Ca and Mg are indeed present.

The approach was to use ungettered argon as a source of oxygen, for reoxidation, using the HT-CSLM setup as described elsewhere.[1,4,8] Normally, the atmosphere in the furnace is maintained by a flow of argon from which oxygen has been gettered with heated copper and magnesium turnings, resulting in an oxygen partial pressure of $10^{-18}$ atm or less (measured at the chamber exit); in ungettered argon, the oxygen activity is much higher (around $10^{-5}$ atm), which should be high enough to cause reoxidation of reactive elements such as Ca or Mg.

## Experimental

The steel composition was 0.04% C, 0.60% Mn, and 0.19% Si based on optical emission spectroscopy; from automated inclusion analysis [using an FEI/ASPEX Explorer scanning electron microscope (SEM)], concentrations of other (bound) elements were estimated as 0.0010% Ca, 0.0005% Mg, and 0.0013% O. Automated inclusion analysis showed the inclusions in the as-received sample to contain CaO, SiO$_2$, and MgO (Fig. 4). In each experiment, a subsample of approximately 0.15 g was placed in an MgO crucible and heated to 1600°C at 500 K/min then held at temperature for 60 s under gettered Ar $(p_{O_2} \sim 10^{-18}$ atm), following which the gas was switched to ungettered Ar $(p_{O_2} \sim 10^{-5}$ atm). Ungettered argon was introduced
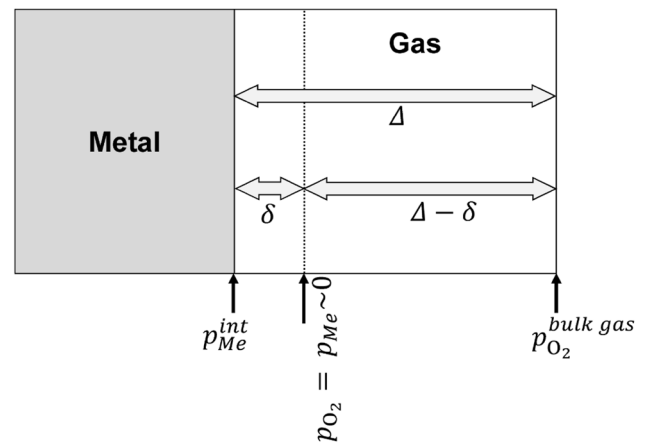


Fig. 5. Schematic of oxygen gettering by vaporized metal within the gas-phase mass transfer boundary layer. $\Delta$ represents the boundary layer thickness in the gas phase, and $\delta$ is the position of the fume-oxygen reaction relative to the metal surface; $p_{Me}^{int}$ is the vapor pressure of metal at the metal–gas interface.

through a bypass line directly linking the argon mass flow controller to the chamber; a computer-triggered valve allowed fast gas switching. Holding and reoxidation times (one sample per condition) were as follows: 10 min at temperature with no reoxidation, exposure to ungettered argon for 2 min, and exposure to ungettered argon for 5 min. Each sample was subsequently cooled to 1300°C at 100 K/min then quenched by turning off the heating lamp. Afterwards, droplet surfaces were examined by

**Table I. Limiting initial gas mass transfer rates of species to or from metal droplet, in the absence of mass transfer limitations in the metal**

| Species | Partial pressure (Pa) | Transfer rate (ppm/s) |
|---|---|---|
| Ca | $1.3 \times 10^{-2}$ | $-6 \times 10^{-4}$ |
| Mg | 47 | $-1.4$ |
| Mn | 31 | $-2.1$ |
| $O_2$ | 1 | 0.062 |

Partial pressures of Ca, Mg, and Mn are for steel–gas equilibrium (calculated with FactSage using the analyzed steel composition), and that of oxygen is in the furnace atmosphere. Transfer rates are expressed relative to the steel mass (positive if pick-up occurs), and each was calculated assuming no effect of the transfer of other species.

SEM (FEI/ASPEX Explorer) at 20 kV; the average chemical composition of the nonmetallic inclusions was measured using energy-dispersive x-ray spectroscopy (EDS).

## Results and Discussion

Upon solidification, the oxide inclusions on the steel surface agglomerated, forming a single particle with diameter of 20–50 $\mu$m. Micrographs and chemical compositions of the inclusion for each sample are shown in Fig. 4. The non-reoxidized sample yielded two different agglomerates—a Ca-silicate and a Mg–silicate—with approximate diameters of 41 $\mu$m, resulting from flotation of Ca- and Mg-containing inclusions. The average chemical composition for this sample was estimated by area-averaging the chemical compositions of the two agglomerates. For the sample held in ungettered argon for 120 s, only one 63-$\mu$m (Mg,Mn)-silicate was detected. Relative to the sample with no reoxidation, there was a *decrease* in overall inclusion area and Mg and Ca concentration, and an increase in Mn and Si concentration. The sample held in ungettered argon for 300 s had a 32-$\mu$m Mn-silicate inclusion (significantly depleted in both Mg and Ca). Unlike what was expected, no increase in Mg and Ca in the oxide phase was observed after exposure of the sample to oxygen-containing argon.

The lack of reoxidation of the sample appears to be the result of evaporation of manganese from the sample; manganese vapor can getter oxygen within the diffusion boundary layer and so prevent oxygen reaching the sample surface (Fig. 5). Turkdogan et al.[17] studied this gettering reaction in detail. Estimated limiting mass transfer rates of manganese and oxygen through the boundary layer—if no interaction with other elements is considered—and the partial pressures used to calculate these rates are summarized in Table I (note that the mass-transfer-limited vaporization rates in Table I are much lower than the surface-limited Langmuir

rate in vacuum[13,14,17]). The high partial pressure of manganese (relative to oxygen) would have resulted in gettering of oxygen by manganese close to the edge of the boundary layer.

Rather than forming more MgO by reoxidation, it appears that in these experiments the MgO concentration in the inclusions decreased, apparently because of Mg vaporization from the metal surface, a mechanism similar to that for the first case considered in this paper.

From these results, it appears not to be possible to effect gas-based reoxidation of reactive elements in Mn-containing steel in HT-CSLM, because evaporated manganese serves as an efficient oxygen getter, precluding oxygen transfer to the metal surface.

## CONCLUSIONS

- The combination of elevated vapor pressure and high surface-to-volume ratio can significantly alter the bulk chemical composition of a HT-CSLM sample with direct impact on nonmetallic inclusion observation.
- For the length scale of HT-CSLM samples, surface tension is the main driver for fluid flow.

## ACKNOWLEDGEMENTS

## REFERENCES

1. S.P.T. Piva, D. Tang, D. Kumar, and P.C. Pistorius, The Minerals, Metals & Materials Society, TMS 2018 *147th Annual Meeting & Exhibition Supplemental Proceedings*, pp. 193-200. The Minerals, Metals & Materials Series. https://doi.org/10.1007/978-3-319-72526-0_18.
2. H. Yin and T. Emi, *Metall. Mater. Trans. B* 34, 483 (2003).
3. S. Spooner, A.N. Assis, J. Warnett, R. Fruehan, M.A. Williams, and S. Sridhar, *Metall. Mater. Trans. B Process. Metall. Mater. Process. Sci.* 47, 2123 (2016).
4. A.N. Assis, J. Warnett, S. Spooner, R.J. Fruehan, M.A. Williams, and S. Sridhar, *Metall. Mater. Trans. B Process. Metall. Mater. Process. Sci.* 46, 568 (2015).
5. P. Misra, V. Chevrier, S. Sridhar, and A.W. Cramb, *Metall. Mater. Trans. B* 31, 1135 (2000).
6. S. Vantilt, B. Coletti, B. Blanpain, J. Fransaer, P. Wollants, and S. Sridhar, *ISIJ Int.* 44, 1 (2004).
7. H. Yin, H. Shibata, T. Emi, and M. Suzuki, *ISIJ Int.* 37, 936 (1997).
8. H. Mu, T. Zhang, L. Yang, R.R. Xavier, R.J. Fruehan, and B.A. Webler, *Metall. Mater. Trans. B Process. Metall. Mater. Process. Sci.* 47, 3375 (2016).
9. E.T. Turkdogan and R.J. Fruehan, in *Making, Shap. Treat. Steel Steelmak. Refin. Vol.*, 11th ed. (The AISE Steel Foundation, Pittsburgh, PA, 1999), p. 37–160.
10. N.J. Themelis, *Transport and Chemical Rate Phenomena* (Yverdon: Gordon and Breach Science, SA, 1995).

11. C.W. Bale, E. Bélisle, P. Chartrand, S.A. Decterov, G. Eriksson, A.E. Gheribi, K. Hack, I.H. Jung, Y.B. Kang, J. Melançon, A.D. Pelton, S. Petersen, C. Robelin, J. Sangster, P. Spencer, and M.A. Van Ende, *CALPHAD: Comput. Coupling Phase Diagrams Thermochem.* 54, 35 (2016).
12. D. Kumar and P.C. Pistorius, *Ceram. Int.* 43, 15478 (2017).
13. P. Grieveson and E.T. Turkdogan, *J. Phys. Chem.* 68, 1547 (1964).
14. R.I.L. Guthrie, *Engineering in Process Metallurgy*, 2nd ed. (New York: Oxford University Press, 1992).
15. N. Verma, P.C. Pistorius, R.J. Fruehan, M.S. Potter, H.G. Oltmann, and E.B. Pretorius, *Metall. Mater. Trans. B Process. Metall. Mater. Process. Sci.* 43, 830 (2012).
16. D. Panda, N. Ross, G. McQuillis, and J. Jenkins, US 2012/0180601 A1 (2012).
17. E.T. Turkdogan, P. Grieveson, L.S. Darken, and C.U. Edgar, *J. Am. Chem. Soc.* 67, 1647 (1963).